Space Science Reviews manuscript No.
(will be inserted by the editor)

The OSIRIS-REx Laser Altimeter (OLA) Investigation and Instrument

M.G. Daly · O.S. Barnouin · C. Dickinson · J. Seabrook · C.L. Johnson · G. Cunningham · T. Haltigin · D. Gaudreau · C. Brunet · I. Aslam · A. Taylor · E.B. Bierhaus · W. Boynton · M. Nolan · D.S. Lauretta

Received: date / Accepted: date

Abstract The Canadian Space Agency (CSA) has contributed to the Origins Spectral Interpretation Resource Identification Security-Regolith Explorer (OSIRIS-REx) spacecraft the OSIRIS-REx Laser Altimeter (OLA). The OSIRIS-REx mission will sample asteroid 101955 Bennu, the first B-type asteroid to be visited by a spacecraft. Bennu is thought to be primitive, carbonaceous, and spectrally most closely related to CI and/or CM meteorites. As a scanning laser altimeter, the OLA instrument will measure the range between the OSIRIS-REx spacecraft and the surface of Bennu to produce digital terrain maps of unprecedented spatial scales for a planetary mission. The digital ter-

M.G. Daly
Centre for Research in Earth and Space Science, York University, Toronto, Ontario, Canada
Tel.: +1-416-736-2100 x22066
Fax: +1-416-736-5626
E-mail: daly@yorku.ca

O.S. Barnouin
Johns Hopkins University Applied Physics Laboratory, Maryland, USA

C. Dickinson, I. Aslam, A. Taylor
MDA, Brampton, Ontario, Canada

J. Seabrook
Centre for Research in Earth and Space Science, York University, Toronto, Ontario, Canada

C.L. Johnson
University of British Columbia, Vancouver, British Columbia, Canada

G. Cunningham
Teledyne Optech, Vaughan, Ontario, Canada

T. Haltigin, D. Gaudreau, C. Brunet
Canadian Space Agency, St. Hubert, Quebec, Canada

E.B. Bierhaus
Lockheed Martin, Denver, Colorado, USA

W. Boynton, M. Nolan, D. Lauretta
University of Arizona, Tucson, Arizona, USA

rain maps produced will have ~7 cm per pixel globally, ~3 cm per pixel at specific sample sites. In addition, OLA data will be used to constrain and refine the spacecraft trajectories. Global maps and highly accurate spacecraft trajectory estimates are critical to infer the internal structure of the asteroid. The global and regional maps also are key to gain new insight into the surface processes acting across Bennu, which inform the selection of the OSIRIS-REx sample site. These, in turn, are essential for understanding the provenance of the regolith sample collected by the OSIRIS-REx spacecraft. The OLA data also are important for quantifying any hazards near the selected OSIRIS-REx sample site and for evaluating the range of tilts at the sampling site for comparison against the capabilities of the sample acquisition device.

Keywords asteroid · lidar · altimeter · OSIRIS-REx · Bennu

Abbreviations

APD	avalanche photodiode
CAT	category
CCA	circuit card assembly
CFD	constant-fraction discriminator
CSA	Canadian Space Agency
EMC	electromagnetic compatibility
HELT	high-energy laser transmitter
LELT	low-energy laser transmitter
LVDS	low voltage differential signaling
MDA	MacDonald, Dettwiler and Associates
OAP	off-axis parabolic mirror
OCAMS	OSIRIS-REx Camera Suite
OLA	OSIRIS-REx Laser Altimeter
OSIRIS-REx	Origins, Spectral Interpretation, Resource Identification, and Security-Regolith Explorer
OTES	OSIRIS-REx Thermal Emission Spectrometer
OVIRS	OSIRIS-REx Visible and Infrared Spectrometer
POST	Power On Self-Test
REXIS	Regolith X-ray Imaging Spectrometer
SBC	single-board computer
SCLK	spacecraft clock
TIM	Time-Interval Meter

1 Introduction

1.1 Mission Overview and the Role of OLA

The objective of Origins, Spectral Interpretation, Resource Identification and Security-Regolith Explorer (OSIRIS-REx) is to return a sample from asteroid 101955 Bennu (Lauretta et al. 2017). The instruments aboard the OSIRIS-REx spacecraft will measure the properties of the asteroid to support the investigation of the geophysical and geochemical state of this B-class asteroid, a subclass within the larger group of C-complex asteroids, that might be organic-rich. At approximately 500 m in mean diameter (Nolan et al. 2013), Bennu is large enough to retain a substantial regolith and is an Apollo asteroid with low inclination (6°). Bennu is the most accessible primitive near-Earth asteroid (Lauretta et al. 2015).

The OSIRIS-REx spacecraft, launched in September 2016, will rendezvous with asteroid 101955 Bennu in 2018. In mid-2021 it will return samples of the asteroid back to the Earth, the first U.S. mission to do so. The returned samples may hold clues to the origin of the solar system and possibly organic molecules that may have seeded life on Earth.

As part of a suite of instruments on the OSIRIS-REx spacecraft, the OSIRIS-REx Laser Altimeter (OLA) is the world's first scanning laser range finder (or lidar) to fly on a planetary mission. Other instruments that make up the scientific payload include cameras (OCAMS) (Rizk 2017), visible and near-infrared spectrometer (OVIRS) (Reuter et al. 2017), a thermal emission spectrometer (OTES) (Christensen et al. 2017), and an X-ray imaging spectrometer (REXIS) (Binzel 2017).

The OLA instrument is very flexible in its ability to collect data because of its long-range and short-range laser transmitters and its scanning mirror. This flexibility is ideal for continuously improving the fidelity of topographical products generated by OLA during the different phases of the OSIRIS-REx mission, as the spacecraft slowly approaches and eventually touches the asteroid. OLA has a series of scientific and mission objectives that can be divided into global and sample-site-scale investigations.

At a global scale, OLA will measure the shape of Bennu to provide insights into the geological origin and evolution of the asteroid by, for example, constraining its bulk density through precise volume measurement. Combined with a carefully undertaken geodesy (McMahon et al. 2017), OLA-based precise ranges, radio science (tracking) data and stereo OCAMS imagery will yield constraints on any global-scale internal heterogeneity of Bennu and hence provide further clues to its origin and subsequent collisional evolution. The OLA-derived asteroid shape, when combined with a mass or gravity measurement, will provide global maps of slopes, geopotential elevation or altitude relative to the asteroid geoid (Scheeres et al. 2016), and vertical roughness that will provide quantitative insights (Cheng et al. 2001; Barnouin-Jha et al. 2008) into how the surface of Bennu evolved subsequent to the formation of the asteroid. Establishing any connection between surface morphological features that possess measurable topography and their spatial relationships to other geological features, such as craters, will provide additional constraints on the interior structure and geophysical evolution of Bennu (Marchi et al. 2015).

Over the sample site (~50 m diameter), OLA will provide detailed information on the geological and geophysical processes that influence the surface regolith at scales (5 cm and greater) relevant to the samples that will be collected. High-resolution (centimeter-scale) spatial measurements of surface topography, slopes, center-of-mass-referenced elevation, and vertical roughness within the sample ellipse will provide data on processes such as surface granular flows (Miyamoto et al. 2007) that may have influenced the regolith distribution on the asteroid. This has implications for the selection of the OSIRIS-REx sample site. OLA data will also be used to assess hazards and safety at any proposed sample site. Specifically, OLA will provide data that will allow the team to measure the geopotential tilt distribution within the sample ellipse and to characterize backscatter roughness at scales below the OLA spot size.

OLA also serves the function of a ranging device by providing precision ranges that are used as part of the data that go into the navigation solutions. These measurements provide increased confidence and faster navigation solutions, thereby improving efficiency, accuracy, and overall mission safety. Additionally, the range measurements allow other instrument teams to improve the scaling of their images or spectral sampling.

1.2 OLA Instrument Overview

The Canadian Space Agency (CSA) contributed OLA to OSIRIS-REx. The instrument was built for CSA by MacDonald, Dettwiler and Associates (MDA), with lidar sensor design and parts provided by subcontractor Teledyne Optech, based in Vaughan, Ontario. The OLA science team is led by York University with support from the University of British Columbia and our United States-based partners.

OLA was developed using heritage components and approaches from previous spaceflight missions. The scanning system and low-energy transmitter share heritage with lidars used to perform the XSS-11 mission (Nimelman et al. 2005). The high-energy transmitter is a modified version of that used in the meteorological lidar on the Phoenix Mars Mission (Whiteway et al. 2008).

These heritage parts were used to constrain the conceptual design in order to reduce development risk. Additional constraints were taken from mission concept of operations discussed in Section 2 and detailed in Lauretta et al. (2017). From these constraints, we developed a set of specifications for the OLA instrument (Table 1). The initial concept was a two-box design with optics, lasers, and detectors in one enclosure, and the main elec-

Table 1 OLA was developed to the following summary set of technical specifications, provided for the High and Low Energy Transmitters as appropriate. Specifications are based on performance to a 3% Lambertian reflector

Specification	High Energy	Low Energy
Maximum Operational Range	≥ 7.4 km	> 0.75 km
Minimum Operational Range	≤ 1.0 km	< 0.475 km (< 200 m goal)
Range Accuracy (1σ)	< 0.5 m	< 0.3 m
Range Precision (1σ)	≤ 0.3 m	≤ 0.04 m
Scanner Field of Regard	±10° (azimuth), ±6° (elevation)	
Scanner Precision	< 100 µrad	< 100 µrad
Laser Divergence (1/e)	200 µrad	100 µrad

tronics in a second one. This approach provided flexibility in accommodating the instrument on the spacecraft.

The maximum required operational range of OLA of ~7 km from the asteroid combined with the 1-mJ-class laser pulse energy and the sensitivity of the XSS-11-derived constant-fraction receiver set the receiver aperture at ~75 mm with a 3 dB link margin. The power-aperture product of the low-energy laser provided a 750 m operational range with a 3 dB link margin. To achieve global coverage of Bennu efficiently, use of the 10 kHz maximum measurement rate of OLA scanning mirror is required. To understand the importance of this system, it should be noted that the ground-track velocity of the spacecraft is of the order of a few cm per second. Therefore, without OLA scanning capability, the measurements per second would be inefficiently placed. Spacecraft motion would improve the situation, but most of the high measurement-rate capability would not be effective.

1.3 Comparison with Previous Planetary Lidars

Table 2 presents a comparative suite of planetary lidars. OLA differs from many of these lidars by its improved range accuracy, resolution, range noise, higher measurement rates and the flexibility provided by its scanning capability. The previous range finders all operated at rates ≤ 50 Hz. OLA will operate at measurement rates of 100 Hz at ranges above 1 km and 10 kHz at lower ranges. Many of these improvements over previous planetary lidars are made practical by the short operational ranges.

The high measurement rate and scanning capability are advantages relative to typical point lidars, especially in the context of a mission where spacecraft ground-track velocities are small. The inclusion of the high measurement rate and scan on OLA make it possible to map large portions of the asteroid surface without spending a substantially long period in orbit to collect the required data (Figure 1). This capability advantage is key to ensure the OSIRIS-REx mission can quickly obtain the ground-based surface measurements needed to validate image-based

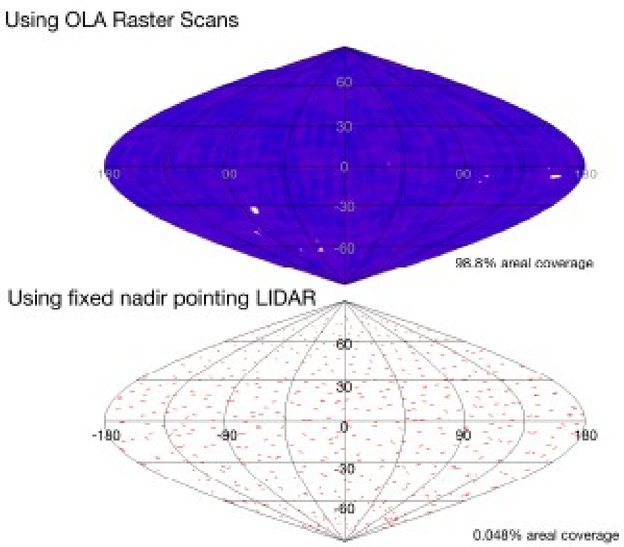

Fig. 1 View of coverage for staring lidar relative to OLA's scanning option for Bennu over same time period and operating with the same duty cycle

Table 2 A comparison of OLA to other planetary lidars. It should be noted that OLA is the only lidar with self-scanning capability. More details can be found in the following: MOLA (Smith et al. 2001); MLA (Cavanaugh et al. 2007); LOLA (Smith et al. 2010, 2017); NLR (Cole et al. 2000); Hayabusa (Mukai et al. 2002); Hayabusa 2 (Mizuno et al. 2016)

Instrument	Target	Range (km)	Accuracy (cm)	Resolution (cm)	Divergence (µrad)	Pulse Energy (mJ)	Pulse Rate (Hz)
MOLA	Mars	200 – 787	100	37.5	420	48	10
MLA	Mercury	< 1500	100	11	55	20	8
LOLA	Moon	< 150	10	[illegible]	100	2.5 (0.5 × 5)	28
NLR	Eros	0.1–300	32	32	100	15.3	1/8, 1, 2, 8
Hayabusa	Itokawa	≤ 50	< 1000	50	1700 × 700	10.5	1
Hayabusa 2	Ryugu	0.03–25	< 5[illegible]	50	2400	15	1
OLA	Bennu	0.01–7	6 (L), 31 (H)	[illegible] (bit), 1.[illegible] (L), 2.6 (H)	100 (L), 200 (H)	0.01 (L), 0.7 (H)	10000 (L), 100 (H)

shape models, and to be able to support hazard assessment and sampling. The scanning capability also has the design advantage of mitigating laser lifetime concerns for the instrument. Such laser lifetime issues tend to be the highest risk item for staring lidars that need to operate for many months (or years) to collect sufficient data from many orbits. In the case of OLA, the scanning capability ensures the instrument achieves all of its scientific objectives within [illegible]00 hours of laser operations.

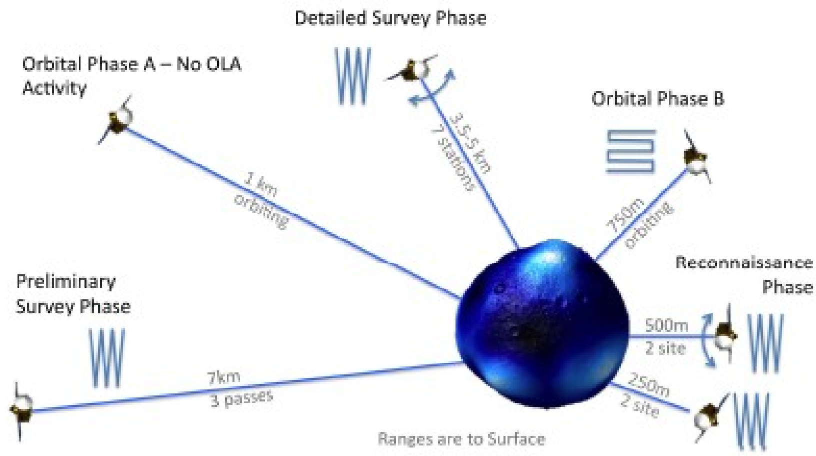

Fig. 2 The OLA operation phases. OLA starts observing 7 km from the surface of the asteroid and was designed to extend to a 525 m reconnaissance sampling site. However, OLA is able to support reconnaissance observations at 250 m and 500 m. Orbital Phase A activity is being considered with polar observations.

2 Operations

2.1 OLA Concept of Operations

The OLA concept of operations is constrained by and designed to be derived from the series of observation phases planned by the OSIRIS-REx mission team (Fig. 2). The mission phases are Preliminary Survey, Orbital Phase A, Detailed Survey, Orbital Phase B, and Reconnaissance. Each of these phases has a different range from the asteroid and distinct spacecraft motions, pointing and local time coverage. See Lauretta et al. (2017) for a detailed description of the mission concept of operations. The operational mission phases for OLA have four distinct ranges and operational methods to characterize the asteroid. Local time is not a constraint for OLA operations. OLA makes use of a highly configurable scanner, and its ability to measure ranges from 7 km and as close as 250 m at two measurement rates, to optimize characterization of the asteroid during these mission phases.

In the Preliminary Survey Phase, the asteroid location relative to the spacecraft is poorly known with respect to the observation geometry. OLA, therefore, is configured in a coarse pushbroom mode in which the scanner operates in a raster manner perpendicular to the spacecraft velocity vector. The scan angle is large enough to accommodate the navigational uncertainties and ensure that Bennu is in the field of view during some of the observation period. The measurement rate is 100 Hz, and ~1-m-diameter footprints are dispersed over the surface so as to ensure that return signals are obtained given the initial spacecraft trajectory uncertainties, but with sufficient density to be able to identify the location of returns in support of OCAMS imaging. As a result, OLA ranges support navigation and provide validation for an asteroid shape model obtained earlier in the mission using camera-based techniques.

As the spacecraft moves closer to the asteroid, the Detailed Survey Phase provides the opportunity for three near-stationary observations over the equator of the asteroid while the asteroid rotates underneath over its 4.3 h period. In this phase, the spacecraft slews in a North–South oscillation with a period of approximately 80 s. In order to maximize the coverage for OLA, an across-swath line-scan was selected. In contrast to the Preliminary Survey Phase, the scan is not sparse but will be configured for 100 Hz measurements every 200 μrads of scanning motion. The ~20 mrad width of each slew is not a critical parameter because a three-swath coverage overlap is typical for OLA in this phase. The Baseball Diamond observations, consisting of two stations in the Northern hemisphere and another in the Southern hemisphere, will allow coverage near the poles (>75° latitude). Each OLA footprint will measure ~1 m in diameter.

In Orbital Phase B, the spacecraft is ~750 m from the surface of the asteroid. This is the main global data-collection phase for OLA, with the goal of enabling the production of a high-resolution global digital terrain map. In this phase, OLA is configured to operate in a similar manner to an imager. Using scan times of two to four minutes and a measurement rate of 10 kHz, OLA will take raster scans of the surface where the spacing is equivalent to the beam divergence, thereby providing contiguous spots, each of ~7.5 cm. A typical scan size will be about 80 m × 80 m on the surface of Bennu. These images are overlapping, enabling a full shape model to be constructed through raster-to-raster registration.

In the Reconnaissance Phase, detailed topography is the required product for sample context and safety. In this phase the spacecraft will slew across-track in support of imaging and spectroscopy. OLA will perform line-scans along the spacecraft's cross-track direction to maximize OLA coverage. The coverage results in substantial overlap with three times spot over-sampling, thereby providing the potential to improve precision through spatial averaging. OLA footprints in this phase measure ~3 cm.

3 OLA Instrument Design

3.1 Design and Performance Overview

OLA consists of two subassemblies (Figure 3): a sensor head (which contains all of the optics, lasers, and circuitry to both drive the lasers and detect return

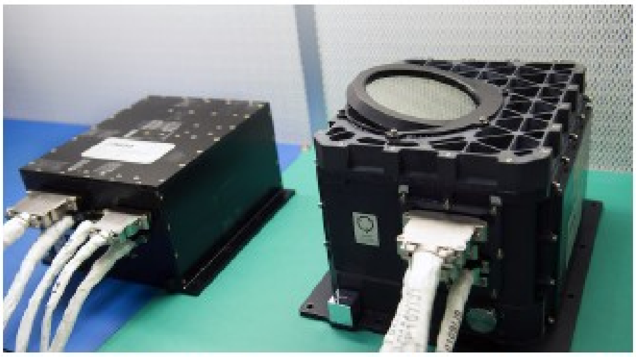

Fig. 3 OLA consists of two subassemblies—The optical head unit (right) and the electronics unit (left)

Table 3 OLA as-built performance and key characteristics. Specifications are based on performance to a 3% Lambertian reflector

Specification	High Energy	Low Energy
Maximum Operational Range	9.0 km	1.2 km
Minimum Operational Range	0.26 km	0.036 km
Range Accuracy (1σ)	< 0.31 m	< 0.06 m
Range Precision (1σ)	< 0.026 m	< 0.011 m
Scanner Field of Regard	±6.7°, ±5.9°	±6.7°, ±5.9°
Scanner Precision	< 20 μrad	< 20 μrad
Laser Divergence (1/e)	200 μrad	100 μrad
False Alarms	$< 10^{-6}$	$< 10^{-6}$
Probability of Detection	> 99.99%	> 99.99%
Clear Aperture	75 mm	75 mm
Pulse Energy	0.7 mJ	10 μJ
Pulse Duration	5 ns	1 ns
Mass - Electronics	7.6 kg	
Mass - Optical Head	13.8 kg	
Power - Nominal	59 W	
Power - Standby	43 W	
Dimensions - Electronics (mm)	265 L × 250 W × 142 H	
Dimensions - Optical Head (mm)	270 L × 320 W × 230 H	

signals) and the final electronics (which contains all of the system avionics such as signal processing, spacecraft communication, and time-of-flight circuitry). The OLA as-built performance is outlined in Table 3. Comparison with Table 2 shows that OLA exceeds its specifications in all but Scanner Field of Regard. During the design phase, a decision was made to increase the mechanical robustness of the scanning system and the scanning range was reduced in one axis from ±10° to ±6°. This change does not compromise the utility of OLA in the mission because the current concept of operations requires no more than ±3° in this axis.

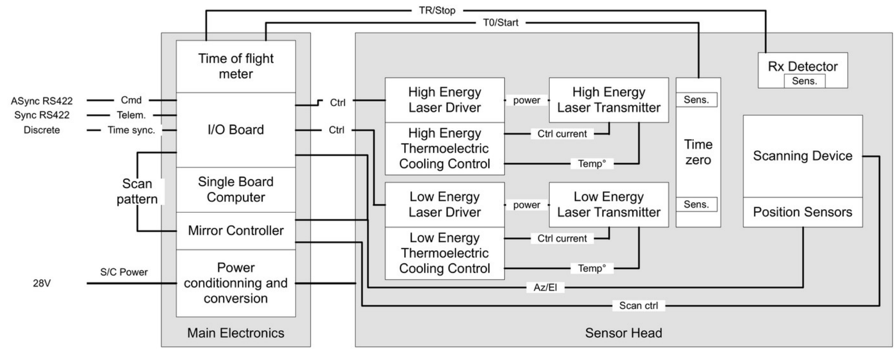

•‘ ’ •‡

‡•™ “ ‘

• • • ’ ¨ ƒ
• • •

… ž Š
Š ƒ • •
• • ƒ
• • • •
‘ ‘ ƒ • ƒ
ƒ • ƒ • • • •
„ ƒ •• ƒ
• ¨™ • •
• Š• -• • € ƒ
•• • • ••
• ƒ … … ƒ • •
• ƒ
• ƒ Ž‘•
• ¨•
• • ••• • • • •
… ƒ • •”‘• •
Š • ƒ • ••
• • • •
ƒ ’ •• •Ÿ
• • • • §
• ’

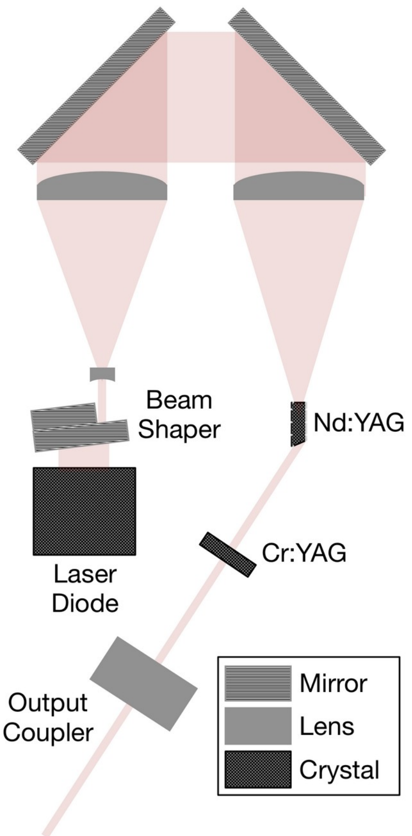
Beam
Shaper
Nd:YAG
Laser
Diode
Cr:YAG
Output
Coupler
Mirror
Lens
Crystal

œ • •‘ •’ ••• ž „ ‡ ‰‡ ‰‡ ˜

• •Œ ¤ • • •
•• • • •

’ ›• •
• • •
• • • •
• ƒ ™•• “• ••• • • • •
• ¡ ƒ • Š • • •
† › •• • • ž •
• † ›•™ •• • • •_™•¨ ••
• • ž
• ƒ ’ ”•
¡ • ƒ • •
••

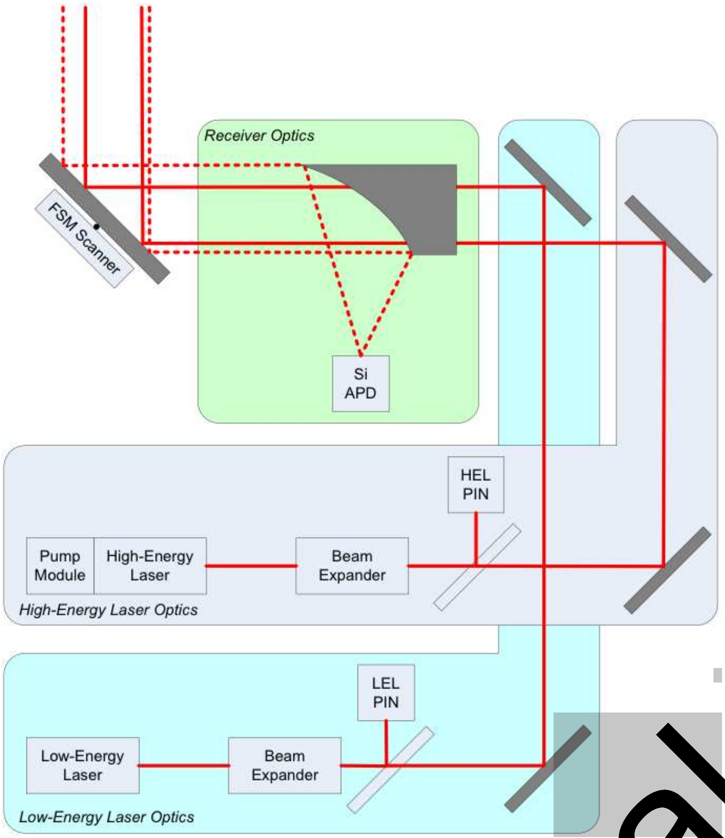

‡ •‡ •‘ ž•‰

• • Š •
• ••, • • • Š
• ƒ • Œ • •• •
• •• • ¤ Š § •
ƒ ¢ ™ ƒ ••
ƒ • ƒ ¤ •
ƒ • • •
• • • • •
• • • • Š ƒ • • Œ
• • „ ƒ •

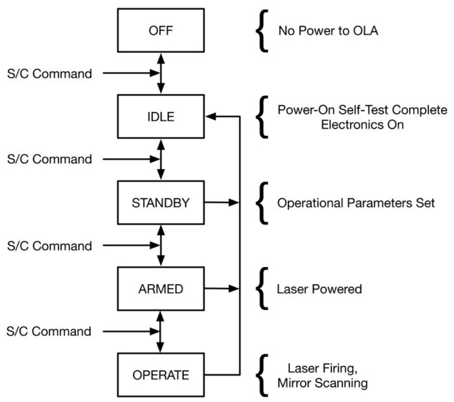

•‘ •‡ • ‡‡ ¡œ

‡•‡ •

• •• •
• • -• •
…“Œ • ƒ Š
¦ ƒ ”¦Š -•- ••
ˆ ««•

•

• • • • • •
• ••
†• • •
§ Œ, , , , ‘
, •
ž , • Ž • Ž,
ƒ , ƒ
• •• Š • • •Ž •
‘• •’ •Ž • •
• ‘••
• Ž , • ‘•
• Š•˜ • • ƒ
• Œ •
• • ••’• • •˜
• Š’ ••
• • ƒ, • Š
• •
, • ƒ •
•

that the parameters are within specified limits. A failure of this check causes a CAT 1 error that logs the error and causes a transition to IDLE.

Upon receiving a command to enter the Standby State, OLA begins heating of critical electrical components to ensure that they are within their operational temperature limits. This nominally takes 5 minutes. This warm-up time is managed operationally through script parameters.

Once OLA is commanded into the Operate State, via a Scan Command with warm-up and scan duration time-out parameters specified, the following steps occur:

Laser Warm-up, no data: To ensure that the OLA laser is operating at peak performance, the entire system is first commanded to operate without data being sent. This is to achieve thermal equilibrium between the thermoelectric coolers and the surrounding. Warm-up time should nominally be 1000 s.

Scan (Operate): Following completion of the warm-up period, OLA proceeds to scan the mirror and to report scan data, provided the scan time-out parameter specified is greater than zero.

Scan Timeout: A scan duration timeout is sent as a parameter within the Scan command, and sets the duration to transition back to the Standby State in the event that:

– The required continuous scan time has expired (for example, a commanded line scan for X minutes).

– The commanded time for a single scan has been exceeded (for example, a single raster scan of known duration).

S/C Monitoring: The spacecraft does not parse OLA science data, with the following two exceptions:

S/C Check One: Once OLA is commanded to the Operate State, the OSIRIS-REx spacecraft checks for the reception of a High Priority data packet. If this check fails, the spacecraft attempts to reinitiate OLA operation (as determined by the command sequence block).

S/C Check Two: The reception of SAFE ME request from OLA to the spacecraft causes OLA to be declared SAFE, and power is removed from the instrument.

The spacecraft can access real-time OLA data that is contained in the science data header. In particular, there is an average range field (based on the 500 measurements for which the header applies) that can be used by the spacecraft for monitoring or for other purposes where 20 Hz measure of range to the surface are needed.

3.3.2 *OLA Scan Configuration*

The main OLA command is Start Scan command. The key parameters for a scan are shown in Table 4. A scan can be made with either the HELT or the LELT. Once the laser transmitter is chosen, the measurement rate is set by the fundamental laser repetition rate. A scan duration provides the length

Table 4 The key fields in OLA Start Scan command

Field	Description	Value
Laser Select	Specify laser	HELT or LELT
Scan Repetition	Enables a single pass through a pattern or repetitive passes	single or continuous
Spot Angular Spacing	Angular separation between adjacent spots	0.05–1.0 mrad
Scan Pattern	Define measurement pattern	Raster, Line or Fixed
Scan Orientation	Direction of fast mirror travel	Azimuth or Elevation
Window Size	Window size (Azimuth or Elevation)	0–340 mrad
Window Center	Center of scan (Azimuth or Elevation)	0–340 mrad
Scan Duration	Duration of scan	0–65,535 s
Receiver Setting	Choose receiver threshold	Nominal or Low
Decimation	Choose Decimation	None, 2×, 10×, 100×, 1000×

of the scan either by pattern repetition (Continuous scan) or by providing a maximum time-out value in Single scan. A lower receiver threshold than the nominal can be set to improve OLA's ranging performance at the expense of an increased false-alarm rate. The majority of the remaining configuration relates to the scanning mirror parameters.

The OLA scanner can be configured in three patterns. A fixed staring pattern is not currently planned for flight, but was implemented to support test configurations. Two operational patterns are a Linear line-scan pattern and a Raster or area-scan pattern. Each of the operational patterns can be configured with their primary axis in the azimuthal or elevation direction. The center of the pattern can be specified with a scan window to allow arbitrary instrument pointing. The scanner speed is set by specifying the angular spacing of spots. This will normally be set at 0.1 mrad for contiguous spots for the LELT. The scan pattern generator interprets this value as the highest mirror velocity. The highest mirror velocity occurs at the center of the scan and the extent of this region varies with the scan pattern as it is limited by the power required to accelerate and decelerate the mirror.

OLA provides the ability to parse and prioritize its data in order to allow management of OLA data volumes, which can be large given OLA's 10 KHz measurement rate. In-FPGA Data Decimation is required, and is achieved through the Scan command with the decimation parameter specified (nominally 2, 10, 100, or 1000) in a scan. Data will then be arranged into Decimated Data (tagged as High Priority Science Data) and Undecimated Data (tagged as Low Priority Science Data). For example, applying a 10-fold decimation scheme would result in 1 scan point in every 10 being put into a High Priority data packet, while all 10 scan points would be put into a Low Priority data packet. The spacecraft has the option to not transmit the Low Priority packet.

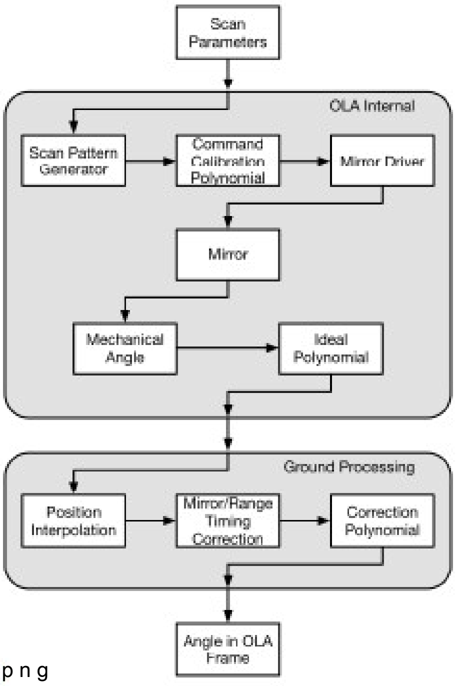

Calibrations.png

Fig. 8 The OLA mirror command and pointing correction approach

3.3.3 *Measurement Data*

The key contents of an OLA measurement point consist of range (mm resolution), time (1 µs resolution), mirror angles (25 µrad resolution), and incoming and outgoing intensities (14-bit values). A data record is shown in Table 5. These values undergo a series of calibrations in the ground processing software (Figures 8 and 9). As shown in Figure 8, OLA has a set of ideal mirror parameters that are polynomials relating commanded mirror driver voltages to desired mirror azimuth and elevation. A similar set of polynomials provide angular position from mirror position voltage readings. A series of ground-based corrections are required to further calibrate these positions. The first of these requires a position interpolation and timing correction to account for timing differences between mirror positions and the range reporting. For OLA, this timing difference is ~130 µs or approximately 3 measurement times when using the LELT and ~650 µs for the HELT. These reported positions are further corrected through 15 coefficient correction polynomials that are functions of the reported azimuthal and elevation coordinates.

Range data corrections (Figure 9) require a range offset that is ~0.75 m and a range-intensity correction. The range-intensity correction is minor (~2 cm) over most of the dynamic range of OLA, as would be expected for a well-designed CFD-based receiver. For lowest 3% of the dynamic range, the

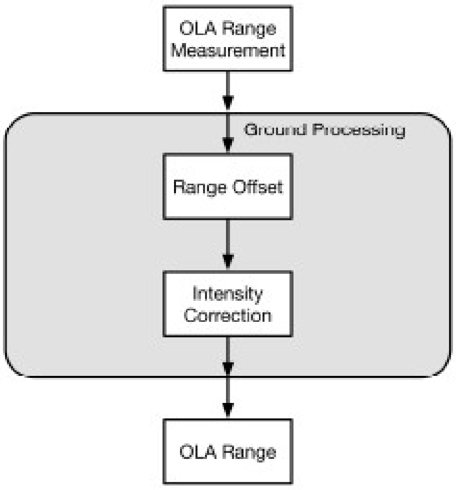

Fig. 9 OLA range correction

Table 5 The key fields in the OLA data record

Field	Description	Value
Scan ID	Unique scan identifier passed back from command	unique integer
Time Sync Fields	Fields required to reference a scan to spacecraft time	various
Range	Integer range in mm	0 to 16 77[illegible]
Azimuth	Measured mirror azimuth	−170 to +1[illegible] mrad (0.025 mrad)
Elevation	Measured mirror elevation	−170 to +[illegible]70 mrad (0.025 mrad)
Intensity t0	Outgoing pulse amplitude	0 to 16383 (arb. units)
Intensity trr	Incoming pulse amplitude	0 to 16383 (arb. units)
Flag	Assessment of valid return	Valid, Overflow, Null

correction increases to as much as 8 cm for the lowest amplitude detection. Additional detail is provided in Section 4.3.

4 Instrument Calibration and Characterization

4.1 OLA Test and Calibration Facilities

OLA test and calibrations took place at three major facilities. The range calibrations, mirror calibrations, and the vibration tests were conducted at MDA's Brampton, Ontario, Canada, facility. The OLA-specific facility includes a calibration wall at a range of 27 m (Figure 10). This wall has a series of surveyed targets to allow the computation of the mirror correction maps. These targets are surveyed relative to a test stand that provides a known, repeatable position for OLA test and calibrations. Survey errors of each target relative to the test stand have been determined by the survey team to be on or-

• •‘ ’œ œ ‰ • œ

• ‡ • • •••œ- • •
’ ••• š • ƒ • •
• • •
¡ ƒ œ ••
• ƒ • •
• ¥Š žƒ
’ ’ • • ¡
• • • ƒ
• • ™† • œ ••
•Ÿ ƒ • ƒ • •
• ‹ • ¥Š
žƒ •
• • ƒ
• ¥Šžƒ •Š Š • ••
• • ••™ Š•• ƒ • •
•‡ • ƒ
• • • • • •
• • ƒ •

¨•™ • …

• •• “• • • •
ƒ • • •
• ’ •

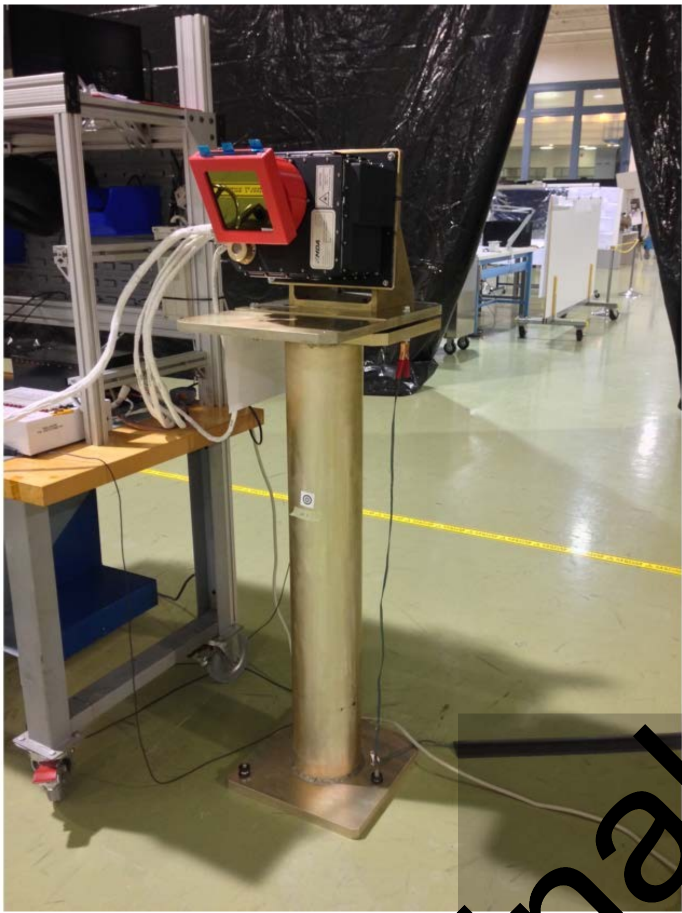

œ •‘ ’

‡•‡•‡•
• • …‘Ÿ €• •
œ• ™• ƒ • ƒ
• • • ••
‚
• •

‘ • “• ••
••‚’ • • • ƒ
ƒ •
Œ• ƒ •
• • • “• ••‚•
• • •• •
• ƒ •

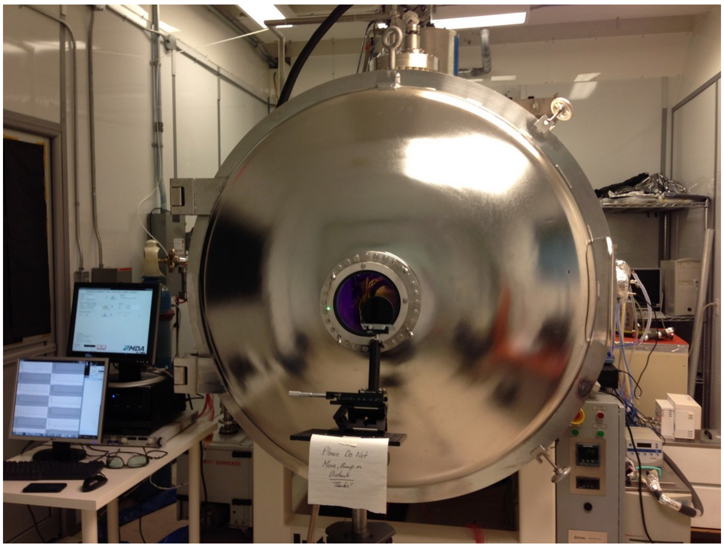

‚ • ‡ ‰‰‡ š•” › •‘ ’ š‰
‚ œœ

• œ ‡ •

ƒ • ™‘
Ž • •¨ • • • •
™‘ •
Œ• ƒ •
• ƒ •• •
• • ƒ •• •
• • ‚ • ƒ
• -• ƒ • Œ
ƒ • ›•

Table 6 The measured deviations between measured and actual target centroids taken during the OLA ambient angular calibration

LELT	Azimuth (μrad)	Elevation (μrad)
Minimum	−119	−172
Maximum	128	150
Standard Deviation	41	47
HELT	**Azimuth (μrad)**	**Elevation (μrad)**
Minimum	−110	−71
Maximum	105	69
Standard Deviation	44	27

4.3 Ambient Range Calibration

Both LELT and HELT range calibrations were performed at the MDA facilities. Range calibrations were done in ambient air using a surveyed target. OLA was mounted to a surveyed stand as shown in Figure 11. The range measurement precision of a single measurement is well characterized by a normal distribution of standard deviation of 1.1 cm for the LELT and 2.6 cm for the HELT. The calibration consisted of determining the range offset between the reported range and the actual range. Although this value could have been integrated into the instrument, the decision was made to incorporate this value into the ground-based calibration pipeline. The range offsets are −869 mm for the LELT and −1269 mm for the HELT.

An additional range-intensity correction was determined using a variable neutral density filter to correct for small range dependence (∼8 cm) on the magnitude of the received signal. This correction is well behaved for the upper 97% of the dynamic range of the instruments (∼2 cm for both the HELT and the LELT). For the lower 3% of the dynamic range, this correction can approach 12 to 15 cm for the smallest detectable signals. This behavior is well-known for constant-fraction discriminators. This correction is implemented in the ground data processing system.

4.4 Additional Range Calibration Considerations

During testing of OLA, it was noted that the LELT exhibits mode-like behavior, in which the T0 signal strength varies shot to shot. This effect was observed on other laser units and appears fundamental to the design of these microchip lasers and is probably due to spatial modes being excited in the laser. Each of these modes has small amplitude and pulse duration difference and therefore requires minor differences in calibration. These modes are interleaved and combined to produce the 10 kHz measurement rate of OLA. In testing, the laser operates stably with this interleaved behavior for many minutes and only rarely sequentially repeats a mode. The data from the range-intensity correction was separated into two modes and analyzed separately. The

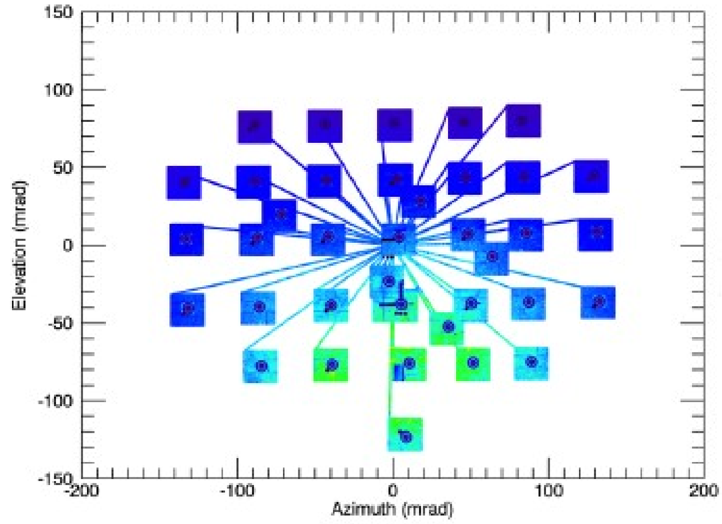

Fig. 14 LELT dynamic scan of the Task Area target wall

consequences of applying these curves is that [illegible] can be higher in the lowest 3% of the instrument's dynamic range. Each scan will have its own range-intensity curve applied in the OLA ground pipeline.

4.5 Long-Range Test

Range tests to validate the long-range performance of OLA and to validate the long-range alignment were conducted at facilities near York University in April 2015. They also provided an example of OLA's scanning capabilities. A top floor (mezzanine) window allowed access to targets of opportunity in the immediate neighborhood (Figure 13); Figure 13 shows the targets used for these tests (inside red circle). The York University smoke stack (referenced as YU Smoke Stack target), at the center of the picture, is roughly 890 m in range from the approximate position of OLA. A student residence, constructed largely of concrete, ~300 m behind the smoke stack (referenced as Building behind YU Smoke Stack target), roughly 1200 m in range from OLA. The foreground foliage and a portion of the top of the building immediately across the street were also scanned during these tests. 3D point clouds of the target with both the LELT and HELT were acquired by rasterscanning the mirror (Figures 15 and 16, respectively). These scans are illustrative of the relative range and resolution performance of the two transmitters.

Data points representative of each target, for both the LELT and HELT, were selected and used together with an analytical range performance model to demonstrate the high-range capability of OLA. The performance matched the prediction within experimental error.

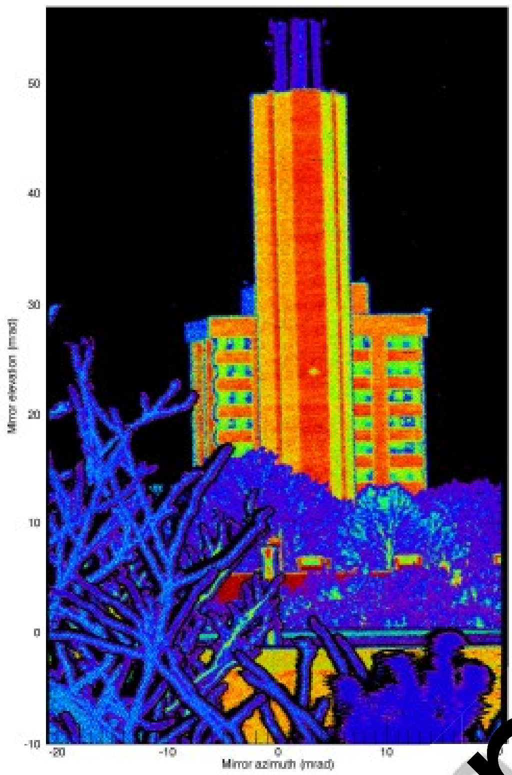

Fig. 15 A LELT raster scan in the mirror frame of reference. The color scale represents the range-corrected return intensity

strengthening the chassis through the design of the optical head unit cover that separates these resonances, and this design change resulted in a successful vibration test. This design change can be seen in Figure 3 where the wall cover is apparent.

OLA thermal vacuum testing consisted of typically shaped cycles with extremes set by mission thermal modeling combined with a single cycle with 5°C plateau temperature steps from −5°C to 30°C. These temperature steps were used to validate OLA specifications over temperature. OLA was mounted near a window at one end of the chamber (Figure 12) in view of a target wall at a 3 m distance with a series of targets of the same size and shape as those used on the calibration at the MDA facilities.

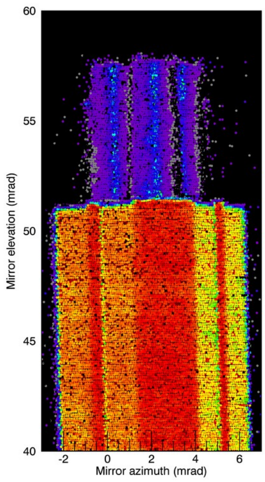

60
55
50
45
40
Mirror elevation (mrad)
-2
0
2
4
6
Mirror azimuth (mrad)

Œ ‘• ‡ ‡ •
• ‡™ ‰

• œ • • ‰ ‡ ‡‰

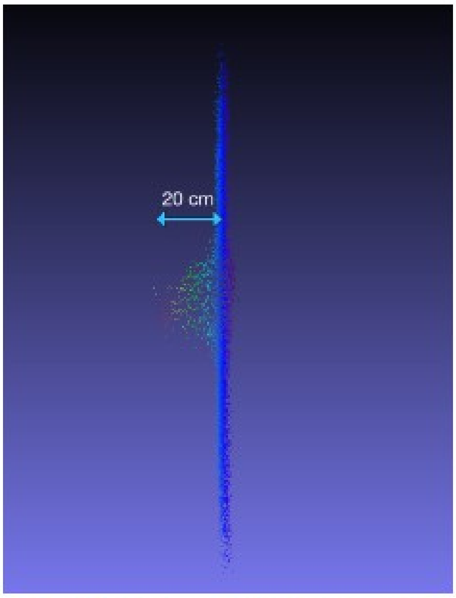

Fig. 18 An OLA point cloud of York University Stack, seen edge on

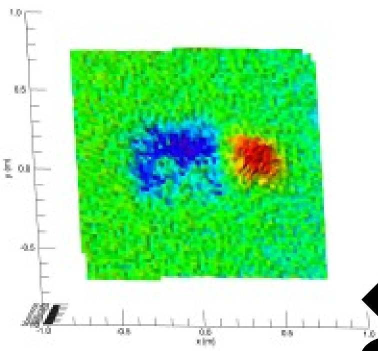

Fig. 19 A Gridded surface showing the aircraft warning lights and security camera scanned by the LELT at a range of 900 m

These targets were used along with an external reference to assess the pointing change of OLA over temperature. There was no significant trend in the elevation axis for the HELT or the LELT with the most showing a linear trend bounded by ~100 μrad change over the 35 °C operational range. In the elevation axis, the performance of the LELT was bounded by a ~250 μrad change and the HELT by a 600 μrad change. All of these changes are roughly linear and well behaved. It should be noted that all OLA observations and their subsequent data processing do not assume absolute pointing stability but only short-term relative pointing stability.

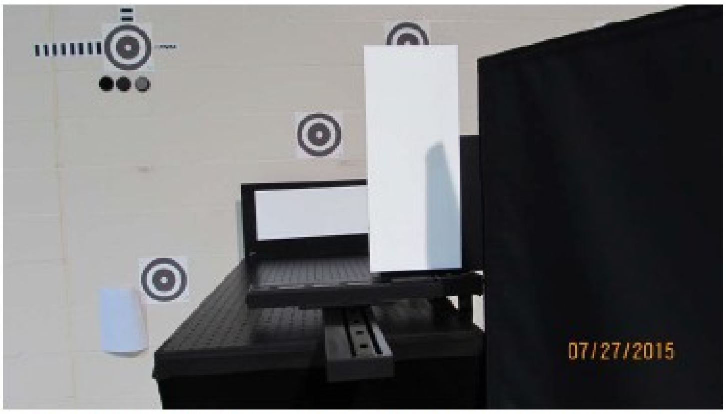

Fig. 20 A photograph of the OLA step characterization experimental apparatus

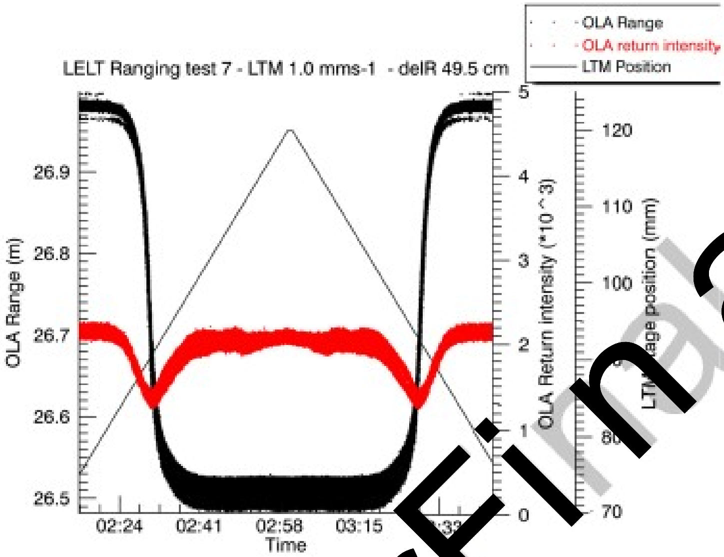

Fig. 21 The OLA step characterization results. The results (thick black lines) demonstrate that for small steps, the reported range transitions gracefully between the two base measurements. The reported range is approximately a weighted average of the ranges of the objects sampled by the incident beam

A more important assessment of pointing for OSIRIS-REx is an evaluation of relative pointing. This can be thought of as a field distortion term and is important because the majority of the OLA analysis is dependent on these data sets collected in minutes and are less dependent on absolute pointing knowledge. Relative pointing was bounded during TVAC tests to be less than 120 µrad in the diagonal over the temperature range. This amounts to 1.2 spot diameters over a typical raster scan field of 1400 spot diameters.

Range measurements changes were shown to be slowly varying and bounded by 4.9 cm for the LELT and 29.5 mm for the HELT. Since the OLA data processing algorithm does not rely on long-term stability but only stability over short spans (i.e., individual swaths in Detailed Survey or single Orbital Phase B scans), it is expected that in-flight topographic will perform approaching that of the inherent instrument noise of 1.1 cm and 2.6 cm.

5 Summary

OLA is a new class of planetary exploration lidar that provides measurement rates 100 to 10,000 times those of previous lidars and provides a flexible scanning system that allows a slow-moving spacecraft to make use of these measurement rates. The increased measurement rate and scan allows OLA to measure the shape of the entire asteroid with unprecedented detail in a short time in orbit. This time advantage is key to ensuring the OSIRIS-REx mission can quickly obtain surface topographic measurements needed to verify prior image-based shape models, and to be able support the hazard assessment critical sampling activity. OLA is expected to map the surface of Bennu with 7 cm precision globally, thereby providing unprecedented topography of an asteroid. OLA also provides precise ranges for spacecraft navigation, thereby adding confidence and improving the efficiency of navigating a spacecraft around this small body.

Acknowledgements There are many important contributors who could not be included in the author list. These contributors include MDA, Teledyne Optech, CSA, York University, University of British Columbia, University of Arizona, Johns Hopkins University Applied Physics Laboratory, Lockheed Martin and NASA Goddard Space Flight Center. The instrument build and Canadian science support was provided by a contract with the Canadian Space Agency. The United States team contribution was supported by National Aeronautics and Space Administration under Contract NNM10AA11C and NNG12FD66C issued through the New Frontiers Program.

References

O.S. Barnouin-Jha, A.F. Cheng, T. Mukai, S. Abe, N. Hirata, R. Nakamura, R.W. Gaskell, J. Saito, B.E. Clark, Small-scale topography of 25143 Itokawa from the Hayabusa laser altimeter. Icarus 198(1), 108–124 (2008)

R. Binzel et al., Regolith x-ray imaging spectrometer (REXIS) aboard the OSIRIS-REx asteroid sample return mission. Space Science Reviews This issue (2017)

J.F. Cavanaugh, J.C. Smith, X. Sun, A.E. Bartels, L. Ramos-Izquierdo, D.J. Krebs, J.F. McGarry, R. Trunzo, A.M. Novo-Gradac, J.L. Britt, J. Karsh, R.B. Katz, A.T. Lukemire, R. Szymkiewicz, D.L. Berry, J.P. Swinski, G.A. Neumann, M.T. Zuber, D.E. Smith, The Mercury Laser Altimeter instrument for the MESSENGER Mission. Space Science Reviews 131(1), 451–479 (2007)

A.F. Cheng, O. Barnouin-Jha, M.T. Zuber, J. Veverka, D.E. Smith, G.A. Neumann, M. Robinson, P. Thomas, J.B. Garvin, S. Murchie, C. Chapman, L. Prockter, Laser Altimetry of Small-Scale Features on 433 Eros from NEAR-Shoemaker. Science 292(5), 488–491 (2001)

P.R. Christensen, V.E. Hamilton, G.L. Mehall, D. Pelham, W. O'Donnell, S. Anwar, H. Bowles, S. Chase, J. Fahlgren, Z. Farkas, T. Fisher, O. James, I. Kubik, I. Lazbin, M. Miner, M. Rassas, L. Schulze, K. Shamordola, T. Tourville, G. West, R. Woodward, D. Lauretta, The OSIRIS-REx thermal emission spectrometer (OTES) instrument. Space Science Reviews This volume (2017)

T.D. Cole, A.F. Cheng, A.R. Reiter, D.E. Smith, M.T. Zuber, Flight characterization of the NEAR Laser Rangefinder. SPIE Vol. 4034, 131–142 (2000)

D.S. Lauretta, A.E. Bartels, M.A. Barucci, E.B. Bierhaus, R.P. Binzel, W.F. Bottke, H. Campins, S.R. Chesley, B.C. Clark, B.E. Clark, E.A. Cloutis, H.C. Connolly, M.K. Crombie, M. Delbó, J.P. Dworkin, J.P. Emery, D.P. Glavin, V.E. Hamilton, C.W. Hergenrother, C.L. Johnson, L.P. Keller, P. Michel, M.C. Nolan, S.A. Sandford, D.J. Scheeres, A.A. Simon, B.M. Sutter, D. Vokrouhlický, K.J. Walsh, The OSIRIS-REx target asteroid (101955) Bennu: Constraints on its physical, geological, and dynamical nature from astronomical observations. Meteoritics & Planetary Science 50(4), 834–849 (2015)

D.S. Lauretta, S.S. Balram-Knutson, E. Beshore, W.V. Boynton, C. Drouet d'Aubigny, D.N. DellaGiustina, H.L. Enos, D.R. Golish, C.W. Hergenrother, E.S. Howell, C.A. Johnson, E.T. Morton, M.C. Nolan, B. Rizk, H.L. Roper, A.E. Bartels, B.J. Bos, J.P. Dworkin, D.E. Highsmith, M.C. Moreau, D.A. Lorenz, L.F. Lim, R. Mink, J.A. Nuth, D.C. Reuter, A.A. Simon, E.B. Bierhaus, B.H. Bryan, R. Ballouz, O.S. Barnouin, R.P. Binzel, W.F. Bottke, V.E. Hamilton, K.J. Walsh, S.R. Chesley, P.R. Christensen, B.E. Clark, H.C. Connolly, M.K. Crombie, M.G. Daly, J.P. Emery, T.J. McCoy, J.W. McMahon, D.J. Scheeres, S. Messenger, K. Nakamura-Messenger, K. Righter, S.A. Sandford, OSIRIS-REx: Sample return from Asteroid (101955) Bennu. Space Science Reviews This Volume (2017)

S. Marchi, C.R. Chapman, O.S. Barnouin, J.E. Richardson, J.-B. Vincent, Cratering on Asteroids, in Asteroids IV, ed. by P. Michel, F.E. DeMeo, W.F. Bottke (University of Arizona Press, Tucson, 2015), pp. 725–744

J.W. McMahon, D.J. Scheeres, S.G. Hesar, D. Farnocchia, S. Chesley, D. Lauretta, The OSIRIS-REx radio science experiment at Bennu. Space Science Reviews This issue (2017)

H. Miyamoto, H. Yano, D.J. Scheeres, S. Abe, O. Barnouin-Jha, A.F. Cheng, H. Demura, R.W. Gaskell, N. Hirata, M. Ishiguro, T. Michikami, A.M. Nakamura, R. Nakamura, J. Saito, S. Sasaki, Regolith Migration and Sorting on Asteroid Itokawa. Science 316(5), 1011 (2007)

T. Mizuno, T. Kase, T. Shiina, M. Mita, N. Namiki, H. Senshu, R. Yamada, H. Noda, H. Kunimori, N. Hirata, F. Terui, Y. Mimasu, Development of the laser altimeter (LIDAR) for Hayabusa2. Space Science Reviews, 1–15 (2016)

T. Mukai, H. Araki, T. Mizuno, N. Hatanaka, A.M. Nakamura, A. Kamei, H. Nakayama, A. Cheng, Detection of mass, shape and surface roughness of target asteroid of MUSES-C by LIDAR. Advances in Space Research 29(8), 1231–1235 (2002)

M. Nimelman, J. Tripp, G. Bailak, J. Bolger, Spaceborne scanning lidar system (SSLS). Proc. SPIE 5798, 73–82 (2005)

M.C. Nolan, C. Magri, E.S. Howell, L.A.M. Benner, J.D. Giorgini, C.W. Hergenrother, R.S. Hudson, D.S. Lauretta, J.-L. Margot, S.J. Ostro, D.J. Scheeres, Shape model and surface properties of the OSIRIS-REx target asteroid (101955) Bennu from radar and lightcurve observations. Icarus 226(1), 629–640 (2013)

S.C. Popescu, Lidar Remote Sensing, *Remote Sensing of Terrestrial Environment* (CRC Press, Boca Raton, FL, 2012), p. 68

D.C. Reuter, A.A. Simon, J. Hair, A. Lunsford, S. Manthripragada, V. Bly, B. Bos, C. Brambora, E. Caldwell, G. Casto, Z. Dolch, P. Finneran, D. Jennings, M. Jhabvala, E. Matson, M. McLelland, W. Roher, T. Sullivan, E. Weigle, Y. Wen, D. Wilson, D.S. Lauretta, The OSIRIS-REx visible and infrared spectrometer (OVIRS): Spectral maps of the asteroid Bennu. Space Sci. Rev. This issue (2017)

B. Rizk, OCAMS: the OSIRIS-REx camera suite. Space Sci. Rev. This issue (2017)

D.J. Scheeres, S.G. Hesar, S. Tardivel, M. Hirabayashi, D. Farnocchia, J.W. McMahon, S.R. Chesley, O. Barnouin, R.P. Binzel, W.F. Bottke, M.G. Daly, J.P. Emery, C.W. Hergenrother, D.S. Lauretta, J.R. Marshall, P. Michel, M.C. Nolan, K.J. Walsh, The geophysical environment of Bennu. Icarus 276, 116–140 (2016)

D.E. Smith, M.T. Zuber, H.V. Frey, J.B. Garvin, J.W. Head, D.O. Muhleman, G.H. Pettengill, R.J. Phillips, S.C. Solomon, H.J. Zwally, W.B. Banerdt, T.C. Duxbury, M.P. Golombek, F.G. Lemoine, G.A. Neumann, D.D. Rowlands, O. Aharonson, P.G. Ford, A.B. Ivanov, C.L. Johnson, P.J. McGovern, J.B. Abshire, R.S. Afzal, X. Sun, Mars Orbiter Laser Altimeter: Experiment summary after the first year of global mapping of Mars. 106(E10), 23689–23722 (2001)

D.E. Smith, M.T. Zuber, G.B. Jackson, J.F. Cavanaugh, G.A. Neumann, H. Riris, X. Sun, R.S. Zellar, C. Coltharp, J. Connelly, R.B. Katz, I. Kleyner, P. Liiva, A. Matuszeski, E.M. Mazarico, J.F. McGarry, A.M. Novo-Gradac, M.N. Ott, C. Peters, L.A. Ramos-Izquierdo, L. Ramsey, D.D. Rowlands, S. Schmidt, V.S. Scott, G.B. Shaw, J.C. Smith, J.-P. Swinski, M.H. Torrence, G. Unger, A.W. Yu, T.W. Zagwodzki, The Lunar Orbiter Laser Altimeter Investigation on the Lunar Reconnaissance Orbiter Mission. Space Science Reviews 150, 209 (2010)

D.E. Smith, M.T. Zuber, G.A. Neumann, E. Mazarico, F.G. Lemoine, J.W. Head III, P.G. Lucey, O. Aharonson, M.S. Robinson, X. Sun, M.H. Torrence, M.K. Barker, J. Oberst, T.C. Duxbury, D. Mao, O.S. Barnouin, K. Jha, D.D. Rowlands, S. Goossens, D. Baker, S. Bauer, P. Gläser, M. Lemelin, M. Rosenburg, M.M. Sori, J. Whitten, T. Mcclanahan, Summary of the results from the lunar orbiter laser altimeter after seven years in lunar orbit. Icarus 283, 70–91 (2017)

J. Whiteway, M. Daly, A. Carswell, T. Duck, C. Dickinson, L. Komguem, C. Cook, Lidar on the Phoenix mission to Mars. J. Geophys. Res., Planets 113(E3) (2008)